Adaptive Multi-Channels Allocation in LoRa Networks

YI YU[1,2], LINA MROUEH[1], (Member, IEEE), DIANE DUCHEMIN[3], (Member, IEEE), CLAIRE GOURSAUD[3], (Member, IEEE), GUILLAUME VIVIER[4], (Senior Member, IEEE), JEAN-MARIE GORCE[3], (Senior Member, IEEE), AND MICHEL TERRÉ[2]

[1]Institut Supérieur d'Electronique de Paris, 75006 Paris, France
[2]Conservatoire National des Arts et Métiers, 75003 Paris, France
[3]Institut National des Sciences Appliquées de Lyon (INSA Lyon), 69100 Villeurbanne, France
[4]Sequans Communications, 92700 Colombes, France

Corresponding author: Lina Mroueh (lina.mroueh@isep.fr)

ABSTRACT In this paper, we consider an IoT dedicated network corresponding to a non licensed LoRa Low Power Wide Area Network. The LoRa network operates in the unlicensed 868 MHz band within a total bandwidth of 1 MHz divided into 8 orthogonal channels of 125 kHz each. Despite the high level of interference, this network offers long range communications in the order of 2 to 5 km in urban areas and 10 to 30 km in rural areas. To efficiently mitigate this high level of interference, LoRa network essentially relies on a Chirp Spread Spectrum (CSS) modulation and on repetition diversity mechanisms. The LoRa CSS modulation spreads the signal within a band of 125 kHz using 6 possible spreading factors (from 7 to 12) to target data rates (starting from 5 kbps for the closest node to 300 bps for the furthest ones). The repetition diversity mechanisms enable the data recovery when the transmission is subject to bad channel conditions or/and high interference levels. Although the CSS modulation protects edge-cell's devices from the high level of interference induced by nodes in the proximity of the gateway, it fails to protect nodes at the edge of a given SF region and several trials are required to recover the packet. In this paper, we propose an adaptive multi-channels allocation policy that attributes multiple adjacent channels of 125 kHz for nodes situated at the edge of SF zones. We study the impact of this adaptive sub-band allocation on the gateways' intensities, the rate distribution and the power consumption. Our results are based on a statistical characterization of the interference in the network as well as the outage probability in a typical cell.

INDEX TERMS Low Power Wide Area Network (LPWAN), LoRa network, Chirp Spread Spectrum modulation, Internet of Things, stochastic geometry, spatial Poisson Point Process.

I. INTRODUCTION

With the massive expansion of the Internet of Things (IoT) application, several dedicated Low Power and Wide Area (LPWA) communications technologies have emerged. A statistical study from Ericsson [1] predicts 34 billion connected devices in 2024 among which 4.5 billion of IoT long range connected devices. To fulfill these massive demand on wireless connectivity, dedicated unlicensed LPWAN, considered as complementary to the licensed ones, have been extensively developed in the last recent years.

In this paper, we focus on the LoRa technology that operates in the unlicensed 868 MHz band [2]–[4] within a total bandwidth of 1 MHz. The frequency band is usually sub-divided into several channels, typically 8 channels of 125 kHz, 4 channels of 250 kHz or 2 channels of 500 kHz. To maximize the success rate of packet transmission, LoRaWAN supports packet repetition and adopts Chirp Spread Spectrum (CSS) modulation that is parametrized by a Spreading Factor (SF). This latter is chosen to adapt the data rate with respect to the radio propagation condition. Depending on the value of SF, a symbol of SF bits is represented by a chirp that occupies a fixed bandwidth, and a chirp duration that increases with SF. The SF value increases with distance and the coverage cell is divided into several SF regions.

The associate editor coordinating the review of this manuscript and approving it for publication was Ayaz Ahmad.

Several experimental and analytic works have addressed the performance of LoRa network in terms of coverage, power consumption and the multi-user network capacity [6]–[8], [10]–[13]. It has been shown that using the highest SF, the LoRa's communication range can reach more than 20 km in line-of-sight environments such as the maritime environment [6], [7]. However, these coverage performances are significantly affected by obstacles and the coverage ranges reduce to few kms in urban and rural environments [6]–[8]. Other experimental setups in [6], [7] show that the device battery life can be increased by tuning the SF, the coding rate and the bandwidth size. Finally, experimental studies were led to evaluate the multi-user capacity of the LoRa gateway [10], [11]. In [11], the authors show that under a packet rate reception of 70%, the gateway supports within 15 mins up to 6000 nodes. The multi-user capacity of the gateway has been also analytically studied in many previous works, including [12], [13] to name but a few. These works generally assess the efficiency of the LoRa communications based on the simplification of strictly orthogonal sequences if they originated from different spreading factors. Indeed, as pointed in [12] signals having different spreading factors can be received simultaneously but, given the co-channel rejection of SF combinations, at the condition that none is received with a much higher power than another. Using the ideal SF orthogonality assumption, the co-spreading factor interference however rapidly limits the scalability of LoRa networks, according to [13]. In this work, the authors found out that in each 125 kHz sub-band, the co-SF interference is the main cause of outage as soon as the number of end devices increases.

In this paper, we propose a statistical modeling of the interference level received in LoRa network considering the intra-SF and cross-SF interference and deduce the outage behavior. To mitigate this high level of interference, LoRa network exploits repetition mechanisms where several trials are performed to recover the packet. This leads to an increased energy consumption and decreases the device battery life. Our goal in this paper is to decrease the number of the trials in the network and hence to improve the energy efficiency. For this, we propose to relax the spectral efficiency by adaptively allocating higher bandwidth depending on the position of the nodes in the cell. To statistically evaluate the network performance, we consider the average statistical behavior where the active sensors and gateways are randomly distributed in a given area according to a random Poisson Point Process (PPP). The randomness of the wireless channel is represented by a mark introduced in the PPP as in [15]–[22]. In a typical LoRa cell, we provide an analytic characterization of the interference and the outage probability distribution in function of the communication range. We derive this probability for both cases of fixed and adaptive sub-band allocation. The expression of the outage depends on the inter-correlation factors between the different spreading factor regions and the multi-band sizes that we also compute in this paper. Based on this outage probability expression, we evaluate the

enhancement in terms of error, rate distribution and power consumption when using multi-channels allocation policy.

The rest of the paper is organized as follows. Section II defines the IoT network, the LoRa Chirp Spectrum modulation and the fixed and adaptive multi-channels allocation. Then, we statistically characterize in Section III the interference in a LoRa network taking into account the inter-correlation factors between the different spreading factor regions and the multi-band sizes. The outage probability within one and multi-trial is deduced in Section IV. Section V explains SF and channels allocation policy. Section VI provides numerical results that assess the analytic ones and compare the numerical performance for the adaptive multichannel allocation to the fixed sub-allocation in terms of outage probability, coverage, rate distribution and power consumption. Finally, Section VII concludes the paper.

II. IoT LoRa NETWORK MODEL
In this section, we describe the system parameters, the Chirp Spectrum Spreading (CSS) modulation as well as the access to the shared medium techniques in LoRa networks.

A. NETWORK PARAMETERS
We consider the uplink of a LoRa network in which a set of active devices Φ_a are distributed in a region $\mathcal{A}$ according to an homogeneous PPP characterized by its intensity λ_a nodes per km^2. We assume no coordination between transmitting devices. The gateways are distributed according to a spatial PPP distribution with intensity λ_b gateways per km^2 and we let Φ_b denote the gateways set. Due to Slivnyak-Mecke Theorem in [16], the statistical behavior in the PPP remains unchanged when adding a gateway at the center of this region. We assume that each sensor node is connected to the nearest gateway. We focus on the typical cell centered at the origin o containing the set of all sensor nodes connected to o. Let $r = |x|$ be the distance between any sensor node x belonging to this typical cell and the origin. The probability distribution function of the distance r is known from [16], [17] and is,

$$f(r) = 2\pi \lambda_b r e^{-\lambda_b \pi r^2}. \tag{1}$$

Due the random spatial distribution of the gateways in the network, the cell coverage radius is a random variable. The maximal coverage radius R_c of the cell is determined with a confidence level of p_c is,

$$R_c = \sqrt{\frac{1}{\pi \lambda_b} \ln\left(\frac{1}{1 - p_c}\right)}. \tag{2}$$

We set $p_c = 99\%$, and we determine λ_b ranges using (2) considering rural and urban environments in Table 1. The sensor nodes transmit with a maximal power of 14 dBm. The sensor nodes and the gateway have omnidirectional antennas with 0 dBi of gain. For a given transmitting node x located at a distance $|x|$ from the typical gateway, the received power at the gateway is,

$$P_r(x) = \alpha |x|^{-\beta} P_t A_f, \tag{3}$$

Parameter	Value
Carrier frequency	868 MHz
Maximum transmit power	14 dBm
Gateway height	30 m
Urban path-loss propagation	$\alpha = 10^{-10.07}$, $\beta = 3.52$
Rural path-loss propagation	$\alpha = 10^{-9.08}$, $\beta = 3.52$
Confidence level	$p_c = 10^{-2}$
Urban gateway intensity λ_b	0.1 to 0.3 gateway per km^2
Urban coverage radius R_c	2 to 5 km
Rural gateway intensity λ_b	0.0015 to 0.015 gateway per km^2
Rural coverage radius R_c	10 to 30 km

where α and β are respectively the attenuation factor and the path-loss exponent derived from the Okumura-Hata model, A_f is the random fading coefficient that is exponentially distributed and P_t the transmission power. In LoRa network, the access to the shared medium is managed by an Aloha protocol. In the absence of a centralized control in the network, this simultaneous access induces significant interference. The gateway receives in addition to its intended attenuated signal, the interference from all other nodes transmitting on the same sub-bandwidth. The network parameters as well as the numerical values of the attenuation factor and the path-loss exponent are summarized in Table 1.

B. CHIRP SPREAD SPECTRUM MODULATION
In a LoRa network in [3], Chirp Spread Spectrum (CSS) modulation is used to spread the signal within a limited bandwidth. This spreading technique protects the edge devices from the devices in the proximity of the network gateway. The spreading factor is dictated by the receiver sensitivity and hence by the threshold communication ranges. A high spreading factor better prevents transmission errors, but at the cost of a reduced data rate. LoRa features 6 possible spreading factors (SF = 7 to 12). Each symbol transmits SF bits, has a time duration T and occupies a bandwidth B such that

$$2^{\text{SF}} = T \times B. \tag{4}$$

A channel coding with a rate $R_c = \frac{4}{5}$ is used, and the spectral efficiency (SE) in bits/s/Hz is,

$$\text{SE(b/s/Hz)} = \frac{R_c \times \text{SF}}{2^{\text{SF}}}.$$

Considering that the chosen SF depends on the distance between the node and the BS, the corresponding SF of a given node x situated at a distance $|x|$ from the gateway o is computed as,

$$\text{SF}(x) = \sum_{\text{SF}_0=7}^{12} \text{SF}_0 \times \mathbb{1}_{\{x \in \mathcal{A}_{\text{SF}}\}}, \tag{5}$$

where

$$\mathcal{A}_{\text{SF}} = \{x \in \Phi_a : \rho_{\text{SF}-1} \leq |x| < \rho_{\text{SF}}\}, \tag{6}$$

and ρ_{SF} is the outer-radius for each SF region with $\rho_6 = 0$. The choice of these outer-radii will be further discussed in Section V.

C. MULTIPLE CHANNELS ALLOCATION
We consider a LoRa network that operates on a frequency 868 MHz within a total allocated bandwidth of 1 MHz. The typical communication bandwidth in values are 125, 250 and 500 kHz in the HF-ISM 900 MHz band. For a given active node $x \in \Phi_a$, we denote by $B_a(x)$ the size of the sub-band on which the transmission occurs. In the following, we describe the fixed allocation strategy and the adaptive multi channels allocation that we introduce in this paper.

1) FIXED SIZE CHANNEL ALLOCATION
For the fixed size channel allocation policy, all the nodes in the network transmit within a fixed sub-band size B_0 chosen among $B_0 = 125$, 250 and 500 kHz, i.e.

$$\forall x \in \Phi_a : B_a(x) = B_0.$$

The total bandwidth of 1 MHz can be divided into $N_m = 8$, 4 or 2 channels. Each sub-band is labeled by an integer between 1 and N_m. The sensor node $x \in \Phi_a$ selects uniformly, before transmission, a random Medium Access Indicator (MAI) $e_{B_0}(x)$ from the set $\mathcal{M} = \{1, \ldots, N_m\}$ as illustrated in Figure 1. The authorized nodes transmit their information within the sub-band labeled by the medium access indicator.
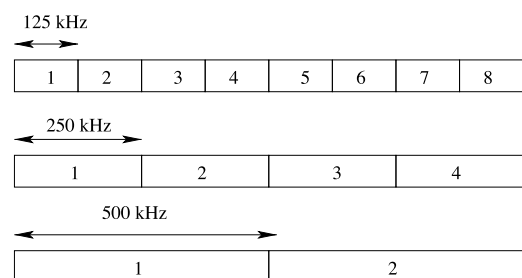

FIGURE 1. Channels labels for different bandwidth size.

Each channel is accessible with the same probability $\text{Prob}\{e_{B_0}(x) = k\} = 1/N_m$, $\forall k$. The intra sub-band interference is induced by nodes that select the same sub-band for transmission. For a given node x transmitting in sub-band $e_{B_0}(x)$, the set of interference contains all nodes transmitting in the same sub-band, i.e.,

$$\Phi_i = \{y \neq x \in \Phi_a : e_{B_0}(y) = e_{B_0}(x)\}. \tag{7}$$

By the thinning theorem [16], the nodes of the set $\Phi_k \cup \{x\}$ are distributed according to a spatial PPP with an homogeneous intensity,

$$\lambda_i(y) = \lambda_a/N_m, \quad \forall y, \tag{8}$$

with $N_m = 8$, 4 or 2 with respect to the size of B_0.

2) ADAPTIVE MULTI-CHANNELS ALLOCATION

Although the CSS modulation protects edge cell devices from the high level of interference induced by nodes in the proximity of the gateway, it fails to protect nodes at the edge of a given SF region. To solve this near-far problem, we propose to decrease the spectral efficiency for the edge nodes of the SF regions. To perform this, we increase progressively, inside each SF region, the size of the bandwidth while keeping the same data rate and same power consumption as shown in Figure 2. Depending on the position of the sensor, the chirps are spread in one, two or four adjacent channels.
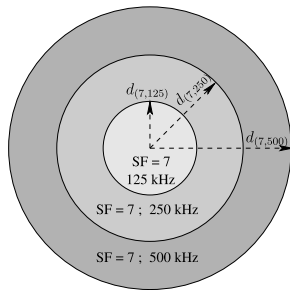

FIGURE 2. Multi-channels allocation within SF zones.

We let $\mathcal{B}_{B_0} = \{x \in \Phi_a : B_a(x) = B_0\}$ be the set of nodes transmitting within a band B_0 and $\mathcal{A}_{SF} \cap \mathcal{B}_{B_0}$ the set of nodes using the same SF and bandwidth size. We denote by $d_{(SF, B_0)}$ the delimiting outer radius of this region. For a given node $x \in \mathcal{A}_{SF}$, the bandwidth allocated to this node using the adaptive multi-sub bands policy is,

$$B_a(x) = \sum_{B_0 \in \{125, 250, 500\}} B_0 \times \mathbb{1}_{\{x \in \mathcal{A}_{SF} \cap \mathcal{B}_{B_0}\}},$$

with

$$\mathcal{A}_{SF} \cap \mathcal{B}_{B_0} = \{x \in \Phi_a : d_{in} \le |x| < d_{(SF, B_0)}\}$$

and

$$d_{in} = \begin{cases} \rho_{SF-1} & B_0 = 125 \text{ kHz}; \\ d_{(SF, B_0/2)} & \text{else.} \end{cases}$$

Based on the delimiting outer-radius $d_{(SF, B_0)}$ with $(SF, B_0) \in \{7, \dots, 12\} \times \{125, 250, 500\}$ and depending on the position of a node in the cell, the SF and the size of the bandwidth are assigned. According to the size of the bandwidth $B_a(x)$, the node x selects randomly and in an uniform way a sub-band index $e_{B_a(x)}(x)$ as illustrated in Figure 1. Our goal is to find the appropriate values of these communications ranges $d_{(SF, B_0)}$ to minimize the average outage probability in the cell. The optimized choice of these outer-radii will be further discussed in Subsection V-B. Note that considering LoRaWAN regional specifications in [4], the devices do not operate with all possible values of the couples (SF, B_0). In this case, the optimization is performed on the authorized combinations of (SF, B_0).

III. STATISTICAL INTERFERENCE CHARACTERIZATION

In the following, we provide a statistical model to characterize the uplink interference computed at a typical gateway situated at the origin. Due to the high ranges in LoRa network, we consider only the intra-cell interference and neglect the inter-cell interference. We consider a given node x situated at distance $r = |x|$ from the typical point and transmitting with a spreading factor $SF(x)$ and within a bandwidth $B_a(x)$. This latter is independent of x in the fixed size case. The interfering set Φ_i is defined in eq. (7) to (18). For a fixed channel allocation and in (10) to (18) for the adaptive channels allocation. The position of a given interferer y in the cell determines its spreading factor $SF(y)$ and the size of its bandwidth $B_a(y)$ in the adaptive allocation case. Depending on the SF and bandwidth of the interferer as well as the intended transmitter ones, the power of the interferer is weighted by a correlation factor denoted by $c(x, y)$. Let I_x define the interference observed at the gateway on an intended transmitter x. The expression of the interference I_x is then,

$$I_x \approx \sum_{y \in \Phi_i} c(x, y) P_r(y) \prod_{z \in \Phi_b} \mathbb{1}_{\{|y| < |z-y|\}}, \quad (9)$$

where $P_r(y)$ being the received power at the gateway o from the transmitter y defined in (3). Note that the right hand side product in (9) is only equal to 1 if the sensor node y is closer to o than all other nodes of the gateways process. In the following, we first characterize the spatial distribution of the interfering nodes. Then, we compute the inter-correlation factor $c(x, y)$ and we characterize the Laplace transform expression of the interference.

A. SPATIAL DISTRIBUTION OF INTERFERING NODES

The set of the interfering nodes depends on the pre-assigned bandwidth $B_a(x)$ on which the intended node x is transmitting. The set of interfering nodes corresponds to

$$\Phi_i = \{y \in \Phi_a : \text{sub-band of y overlap with sub-band of x}\}.$$

In the following, we detail three possible cases.

1) CASE 1: $B_a(x) = 125$ kHz

Given a device transmitting on the band $B_a(x) = 125$ kHz say with $e_{125}(x) = 3$ for example. The interference is generated by: (i) devices with band 125 kHz transmitting on sub-band 3 in Figure 1, (ii) devices with band 250 kHz transmitting on sub-band 2 in Figure 1 and (iii) devices with band 500 kHz transmitting on sub-band 1 in Figure 1. The set of interfering nodes Φ_i can be written as the union of three subsets such that $\Phi_i = \Phi_{i,1} \cup \Phi_{i,2} \cup \Phi_{i,3}$, with

$$\Phi_{i,1} = \{y \ne x \in \mathcal{B}_{125} : e_{125}(y) = e_{125}(x)\}, \quad (10)$$

$$\Phi_{i,2} = \{y \in \mathcal{B}_{250} : 2e_{250}(y) - 1 = e_{125}(x)\}$$
$$\cup \{y \in \mathcal{B}_{250} : 2e_{250}(y) = e_{125}(x)\} \quad (11)$$

$$\Phi_{i,3} = \{y \in \mathcal{B}_{500} : 4e_{500}(y) - 3 = e_{125}(x)\}$$
$$\cup \{y \in \mathcal{B}_{500} : 4e_{500}(y) - 2 = e_{125}(x)\}$$
$$\cup \{y \in \mathcal{B}_{500} : 4e_{500}(y) - 1 = e_{125}(x)\}$$
$$\cup \{y \in \mathcal{B}_{500} : 4e_{500}(y) = e_{125}(x)\} \quad (12)$$

Note that the intensity of interfering nodes in $\Phi_{i,1}$ is $\lambda_a/8$, in $\Phi_{i,2}$ is $\lambda_a/4$ and in $\Phi_{i,3}$ is $\lambda_a/2$.

2) CASE 2: $B_\sigma(x) = 250$ kHz

In a similar way, assuming $B_a(x) = 250$ kHz, the interference set Φ_i is $\Phi_i = \Phi_{i,1} \cup \Phi_{i,2} \cup \Phi_{i,3}$, with

$$\Phi_{i,1} = \{y \in \mathcal{B}_{125} : e_{125}(y) = 2e_{250}(x)\},$$
$$\cup \{y \in \mathcal{B}_{125} : e_{125}(y) = 2e_{250}(x) - 1\} \quad (13)$$
$$\Phi_{i,2} = \{y \neq x \in \mathcal{B}_{250} : e_{250}(y) = e_{250}(x)\} \quad (14)$$
$$\Phi_{i,3} = \{y \in \mathcal{B}_{500} : 2e_{500}(y) - 1 = e_{250}(x)\}$$
$$\cup \{y \in \mathcal{B}_{500} : 2e_{500}(y) = e_{250}(x)\} \quad (15)$$

The intensity of interfering nodes in $\Phi_{i,1}$ is $2\lambda_a/8 = \lambda_a/4$, in $\Phi_{i,2}$ is $\lambda_a/4$ and in $\Phi_{i,3}$ is $\lambda_a/2$.

3) CASE 3: $B_\sigma(x) = 500$ kHz

For the case with $B_a(x) = 500$ kHz, the interference set $\Phi_i = \Phi_{i,1} \cup \Phi_{i,2} \cup \Phi_{i,3}$, with

$$\Phi_{i,1} = \{y \in \mathcal{B}_{125} : e_{125}(y) = 4e_{500}(x) - 3\},$$
$$\cup \{y \in \mathcal{B}_{125} : e_{125}(y) = 4\,e_{500}(x) - 2\}$$
$$\cup \{y \in \mathcal{B}_{125} : e_{125}(y) = 4\,e_{500}(x) - 1\}$$
$$\cup \{y \in \mathcal{B}_{125} : e_{125}(y) = 4\,e_{500}(x)\} \quad (16)$$
$$\Phi_{i,2} = \{y \in \mathcal{B}_{250} : e_{250}(y) = 2e_{500}(x) - 1\}$$
$$\cup \{y \in \mathcal{B}_{250} : e_{250}(y) = 2\,e_{500}(x)\} \quad (17)$$
$$\Phi_{i,3} = \{y \neq x \in \mathcal{B}_{500} : e_{500}(y) = e_{500}(x)\} \quad (18)$$

The intensity of interfering nodes in $\Phi_{i,1}$ is $4 \times \lambda_a/8 = \lambda_a/2$, in $\Phi_{i,2}$ is $2\lambda_a/4 = \lambda_a/2$ and in $\Phi_{i,3}$ is $\lambda_a/2$.

HETEROGENEOUS INTERFERING NODES DISTRIBUTION

Considering the three above mentioned different cases, the set of interfering nodes on an intended node x with assigned sub-band size B_x, is distributed as a spatial PPP with heterogeneous distribution that depends on x and on the position of y and is given by,

$$\lambda_{i,x}(y) = \sum_{B_y \in \{125,250,500\}} \Lambda(B_y, B_x)\mathbb{1}_{\{y \in \mathcal{B}_{B_y}|x \in \mathcal{B}_{B_x}\}},$$

The values of $\Lambda(B_x, B_y)$ are detailed in Table 2 and can be deduced by considering the intensity of the sets detailed in (10) to (18).

TABLE 2. Intensity $\Lambda(B_y, B_x)$.

B_y \ B_x	125	250	500
125	$\lambda_a/8$	$\lambda_a/4$	$\lambda_a/2$
250	$\lambda_a/4$	$\lambda_a/4$	$\lambda_a/2$
500	$\lambda_a/2$	$\lambda_a/2$	$\lambda_a/2$

B. INTER-CORRELATION FACTOR COMPUTATION

The CSS modulation is based on chirp signal (obtained through a continuously varying carrier frequency [23]). A single LoRa chirp codes up to SF = 12 bits. To do so, during one chirp period, a specific frequency trajectory is defined for each of the 2^{SF} symbols. This is done by shifting the chirp based on the symbol value, so that the lowest frequency is observed at time $\frac{k}{B}$ where k is the symbol numerical value, and B is the sub-bandwidth. This introduces a sharp edge in the instantaneous frequency trajectory. Let us consider a transmitting node interfering with the intended signal. The expression for the instantaneous frequency of the interfering coded chirp is thus:

$$f_{cc}^{(k)}(t) = \begin{cases} \frac{B}{T}\left(t - \frac{k}{B}\right) + B & \text{if } -\frac{T}{2} \leq t \leq \frac{k}{B} \\ \frac{B}{T}\left(t - \frac{k}{B}\right) & \text{if } \frac{k}{B} \leq t \leq \frac{T}{2}. \end{cases} \quad (19)$$

with $0 \leq k \leq 2^{SF} - 1$. At the receiver side, the received signal is multiplied with the raw down-chirp (supposedly perfectly synchronized) related to the desired user parameters. The instantaneous frequency becomes:

$$f_p(t) = \left(\left(\frac{B}{T} - \frac{B_0}{T_0}\right) \times t - \frac{k}{T} + B\right)\mathbb{1}_{\{-\frac{T}{2} \leq t \leq \frac{k}{B}\}}$$
$$+ \left(\left(\frac{B}{T} - \frac{B_0}{T_0}\right) \times t - \frac{k}{T}\right)\mathbb{1}_{\{\frac{k}{B} \leq t \leq \frac{T}{2}\}}$$

This signal is then sampled at B_0 Hz, leading to 2^{SF_0} samples such that

$$s(n) = A\exp\left(j2\pi \int_0^{\frac{n \cdot T_0}{2^{SF_0}}} \text{mod } (f_p(t), B_0)\, dt\right), \quad 1 \leq n \leq 2^{SF_0}. \quad (20)$$

with A the amplitude coefficient which aggregates the effects of the transmitted power, channel losses, and circuit. The samples are processed with a Fast Fourier Transform (FFT) of 2^{SF_0} size. The generated contribution, which depends on the initial parameters of the encoded chirp is thus given by:

$$S_m(\text{SF}, B) = \max\left(\text{FFT}\left[s(1), \ldots, s\left(2^{SF_0}\right)\right]\right). \quad (21)$$

We can finally deduce the inter-correlation factor, by comparing the contribution of the interferer y with $\text{SF}(y) = \text{SF}_y$ and $B_a(y) = B_y$ to the desired user's x using $\text{SF}(x) = \text{SF}_x$ and $B_a(x) = B_x$ such that,

$$c(x, y) = \frac{S_m(\text{SF}_x, B_x)}{S_m(\text{SF}_y, B_y)}. \quad (22)$$

Note that this inter-correlation factor depends on the parameters $(\text{SF}_x, B_x, \text{SF}_y, B_y)$, and is denoted in the following as

$$c(x, y) = c_{\{\text{SF}_x, B_x, \text{SF}_y, B_y\}}.$$

Besides, the spreading factor SF can vary from 7 to 12. Tables 4 and 5 provide all numerical data obtained for all these cases regardless of the network topology and activity.

C. INTERFERENCE LAPLACE TRANSFORM COMPUTATION

Let I_x be the random power of interference on the signal of a given transmitter x situated at a distance r from the typical o and transmitting with $\mathrm{SF}(x) = \mathrm{SF}_x$ and within a sub-band $B_a(x) = B_x$. The Laplace transform of the interference I_x computed for $s \in \mathbb{R}$ is

$$\mathcal{L}_{I_x}(s) = \mathbb{E}\left[e^{-sI_x}\right].$$

Considering the cases of a fixed sub-band allocation and adaptive multi-band allocation, we have derived in Appendix VII-A1 and VII-A2 the expression of the Laplace transform. The main results are summarized as follows.

1) FIXED SUB-BAND ALLOCATION
In this case, the sub-band is fixed and is allocated independently of the node position *i.e.* $B_a(y) = B_a(x) = B_0$. Independently of the node x position in the cell, the interferer is distributed in a spatial PPP with intensity λ_a/N_m. Given a sensor node position x in the typical cell, the expression of the interference Laplace transform is

$$\mathcal{L}_{I_x}(s) = \exp\left(-\frac{\lambda_a}{N_m} 2\pi \sum_{\mathrm{SF}=7}^{12} \kappa(s)\right). \quad (23)$$

with

$$\kappa(s) = \int_{\rho_{\mathrm{SF}-7}}^{\rho_{\mathrm{SF}-6}} \frac{s\omega P_t \alpha r^{-\beta}}{s\omega P_t \alpha r^{-\beta} + 1} \, r \, e^{-\lambda_b \pi r^2} \, dr. \quad (24)$$

and $\omega = c_{\{\mathrm{SF}_x, B_0, \mathrm{SF}_y, B_0\}}$ is the inter-correlation factor weight.
Proof: See Appendix VII-A1 ∎

2) ADAPTIVE MULTI CHANNELS ALLOCATION
The expression of the Laplace transform of the interference on a transmitter x depends upon the size of its allocated bandwidth $B_a(x) = B_x$, and is given by,

$$\mathcal{L}_{I_x}(s) = \exp\left(-2\pi g(x)\right), \quad (25)$$

with

$$g(x) = \sum_{\mathrm{SF}=7}^{12} \sum_{B_y \in \{125, 250, 500\}} \xi(s), \quad (26)$$

and

$$\xi(s) = \int_{y \in \mathcal{A}_{\mathrm{SF}} \cap \mathcal{B}_{B_y}} \Lambda(B_y, B_x) \frac{s\omega P_t \alpha r^{-\beta}}{s\omega P_t \alpha r^{-\beta} + 1} \, r \, e^{-\lambda_b \pi r^2} \, dr, \quad (27)$$

such that $\omega = c_{\{\mathrm{SF}_x, B_x, \mathrm{SF}_y, B_y\}}$ and $r = |y|$.
Proof: See Appendix VII-A2 ∎

IV. OUTAGE PROBABILITY COMPUTATION

For a given transmitter x situated at a distance $r = |x|$ from the typical gateway o and transmitting with $\mathrm{SF}(x) = \mathrm{SF}_x$ within a sub-band $B_a(x) = B_x$, the received SINR(x) from a sensor node x at a typical gateway point o is

$$\mathrm{SINR}(x) \approx \frac{P_r(x)}{P_n + I_x} \quad (28)$$

where $P_r(x)$ is the received power in (3), P_n is the thermal noise power, I_x is the interference power and A_f the equivalent fading coefficient that is exponentially distributed. There will be a failure in the transmission if the value of SINR is less than a given threshold. This threshold is determined in order to ensure a target symbol error rate. For the fixed or the adaptive sub-band allocation, the failure probability is,

$$\mathbb{P}_{\mathrm{out}}(r) = \mathrm{Prob}\{\mathrm{SINR}(x) < \gamma_{(\mathrm{SF}_x, B_x)}\},$$

with $\gamma_{(\mathrm{SF}_x, B_x)}$ being the required threshold values according to (SF_x, B_x).

A. THRESHOLD VALUES
The analytical expression of symbol error rate using the LoRa PHY layer has been derived in [24] and compared to the simulation ones. These symbol error probabilities were computed for different spectral efficiencies using spreading factors SF = 7 to 12. By targeting a symbol error probability of 10^{-4}, we have deduced from [24] the values of $\gamma_{(\mathrm{SF}, 125)}$ in Table 3. When targeting the same data rate with a larger bandwidth than 125 kHz, the time dedicated to transmit the SF bits contained within a chirp should remain unchanged. Spreading the signal on a larger bandwidth of 250 or 500 kHz naturally decreases the chirp duration compared to the case of 125 kHz. Using (4), the chirp duration reduces to half in the case of 250 kHz and to the quarter in the case of 500 compared to the chirp duration in 125 kHz. To keep the same data rate despite the reduced chirp duration, we propose to repeat the same chirp twice for the case with 250 kHz and four times with 500 kHz. In each trial, the spectral efficiency for a given SF remains the same as in the case of 125 kHz. The chirp is completely lost if it is impossible to recover it in all the trials. Based on this multi-trial transmission when considering multi-bands allocations within the duration of a packet of SF bits, we have deduced from [24] the values of $\gamma_{(\mathrm{SF}, 250)}$ and $\gamma_{(\mathrm{SF}, 500)}$ listed in Table 3.

TABLE 3. Threshold $\gamma_{(\mathrm{SF}, B_x)}$ in dB.

B_x \ SF	7	8	9	10	11	12
125	-7.5	-10	-12.5	-15	-18	-21
250	-9	-12	-14.5	-17	-20	-23
500	-11	-13.8	-16.5	-19	-21.8	-25

B. OUTAGE PROBABILITY
Using the distribution of the exponential distribution of the fading, the expression of the probability simplifies to

$$\mathbb{P}_{\mathrm{out}}(r) \approx 1 - \mathcal{L}_{P_n}(s)\mathcal{L}_{I_x}(s), \quad (29)$$

with

$$s = \frac{\gamma_{(\mathrm{SF}_x, B_x)}}{\alpha r^{-\beta} P_t}.$$

TABLE 4. Inter-correlation factors $c_{\{SF_x, B_x, SF_y, B_y\}}$ in dB, x is the intended device and y the interfering device.

SF$_x$ / B$_x$ \ SF$_y$ / B$_y$		7			8			9		
		125	250	500	125	250	500	125	250	500
7	125	0	21.07	21.07	16.67	21.07	21.07	18.20	0	21.07
	250	12.41	0	21.07	13.33	16.67	21.07	13.66	18.20	0
	500	13.80	12.41	0	13.51	13.33	16.67	13.73	13.66	18.20
8	125	24.08	24.08	24.08	0	24.08	24.08	19.70	24.08	24.08
	250	19.70	24.08	24.08	15.42	0	24.08	16.23	19.70	24.08
	500	16.38	19.70	24.08	16.46	15.42	0	16.57	16.23	19.70
9	125	27.09	27.09	27.09	27.09	27.09	27.09	0	27.09	27.09
	250	6.02	27.09	27.09	22.71	27.09	27.09	18.39	0	27.09
	500	24.60	6.02	27.09	18.96	22.71	27.09	19.45	18.39	0
10	125	30.10	30.10	30.10	30.10	30.10	30.10	30.10	30.10	30.10
	250	27.51	30.10	30.10	6.02	30.10	30.10	25.73	30.10	30.10
	500	25.72	27.51	30.10	27.57	6.02	30.10	22.15	25.73	30.10
11	125	33.11	33.11	33.11	33.11	33.11	33.11	33.11	33.11	33.11
	250	28.30	33.11	33.11	30.55	33.11	33.11	6.020	33.11	33.11
	500	12.04	28.30	33.11	28.73	30.55	33.11	30.56	6.02	33.11
12	125	36.12	36.12	36.12	36.12	36.12	36.12	36.12	36.12	36.12
	250	30.92	36.12	36.12	31.49	36.12	36.12	33.57	36.12	36.12
	500	33.53	30.92	36.12	12.04	31.49	36.12	31.75	33.57	36.12

The Laplace transform interference expressions $\mathcal{L}_I(s)$ are given in (23) for the fixed band case and in (25) for the adaptive one. The noise Laplace transform $\mathcal{L}_{P_n}(s)$ is computed as,

$$\mathcal{L}_{P_n}(s) = \frac{1}{sN_o\,\mathrm{B}_x + 1},$$

and $N_o = 10^{-17.4}$ mW/Hz. Considering a single trial, the average outage probability in the typical cell is then,

$$\bar{\mathbb{P}}_{\text{out}} = \int \mathbb{P}_{\text{out}}(r)f(r)dr.$$

For a multi-trial transmission with L number of replications, which is the case in a LoRa network, the transmission fails if no successful transmission occurs during the L trials. The average outage probability is

$$\bar{\mathbb{P}}_{\text{out}}(L) = \int \mathbb{P}_{\text{out}}(r)^L f(r)dr. \tag{30}$$

V. SF AND CHANNEL ALLOCATION POLICY
In this section, we detail the SF and sub-band allocation policy that we used to delimit the outer-radii of the regions with nodes sharing the same SF and the same band B_x i.e. $\mathcal{A}_{\text{SF}} \cap \mathcal{B}_{B_x}$.

A. SF ALLOCATION POLICY
The outer-radii of SF zones depends on the power consumption of the devices as well as the intensity of gateways in the network and consequently the average coverage radius

R_c in (2). The nodes situated at a distance less than R_c are assigned to the CSS with spreading factor from 7 to 11, and we set ρ_{11} to R_c i.e. $\rho_{11} = R_c$. The SF $= 12$ is left for devices tuated at a distance above R_c. One can compute the path-loss at the distance R_c and deduce the maximal required path-loss. Based on the coefficients of the Okumura Hata model in Table 1, the maximal path-loss in dB denoted $\text{PL}_{\text{max}}^{(11)}$ in the zone with SF $= 11$ is computed as,

$$\text{PL}_{\text{max}}^{(11)} = 10\log_{10}\left(\alpha R_c^{-\beta}\right).$$

As we can notice from Table 3, there is a gap of

$$\Delta\gamma_{(\text{SF}, B_x)} = \gamma_{(\text{SF}, B_x)} - \gamma_{(\text{SF}+1, B_x)} = \Delta\gamma_{\text{SF}}, \quad \forall B_x$$

when decreasing the spreading factor. The maximal path-loss in the other SF regions is then deduced as,

$$\text{PL}_{\text{max}}^{(\text{SF})} = \text{PL}_{\text{max}}^{(\text{SF}+1)} - \Delta\gamma_{\text{SF}} \quad 7 \leq \text{SF} \leq 10.$$

Based on the Okumura Hata model in Table 1, the outer-radius of each SF region can be computed accordingly.

B. MULTIPLE CHANNELS ALLOCATION POLICY
Given the choice of the SF outer-radius, we allocate the channels to minimize the average outage probability in the cell. The delimiting outer-radius $d_{(\text{SF}, B_x)}$ of the $\mathcal{A}_{\text{SF}} \cap \mathcal{B}_{B_x}$ region is expressed in function of the conditional probability $p_{(B_x|\text{SF})}$ that we define as,

$$p_{(B_x|\text{SF})} \triangleq \text{Prob}\left\{x \in \mathcal{B}_{B_x} \big| x \in \mathcal{A}_{\text{SF}}\right\}. \tag{31}$$

TABLE 5. Inter-correlation values $c_{(SF_x,B_x,SF_y,B_y)}$ in dB, x is the intended device and y the interfering device.

SF$_x$ / B$_x$	B$_y$	SF$_y$ 10			11			12		
		125	250	500	125	250	500	125	250	500
7	125	18.62	16.45	18.51	18.70	18.14	0	18.65	18.60	16.46
	250	14.01	18.62	16.46	13.98	18.70	18.15	13.74	18.65	18.60
	500	13.87	14.01	18.62	14.19	13.98	18.7	13.9	13.74	18.65
8	125	21.27	0	24.08	21.75	19.54	21.52	21.82	21.21	0
	250	16.65	21.27	0	16.90	21.75	19.54	17.00	21.82	21.21
	500	16.60	16.65	21.27	16.61	16.9	21.75	16.75	17.00	21.82
9	125	22.71	27.09	27.09	24.34	0	27.09	24.85	22.60	24.54
	250	19.17	22.71	27.09	19.66	24.34	0	19.79	24.85	22.60
	500	19.76	19.17	22.71	19.75	19.66	24.34	19.68	19.79	24.85
10	125	0	30.10	30.10	25.73	30.10	30.10	27.38	0	30.10
	250	21.43	0	30.10	22.08	25.73	30.10	22.56	27.39	0
	500	22.44	21.43	0	22.79	22.08	30.10	22.60	22.56	27.39
11	125	33.11	33.11	33.11	0	33.11	33.11	28.73	33.11	33.11
	250	28.73	33.11	33.11	24.44	0	33.11	25.10	28.73	33.11
	500	25.13	28.73	33.11	25.42	24.44	33.11	25.68	25.10	28.73
12	125	36.12	36.12	36.12	36.12	36.12	36.12	0	36.12	36.12
	250	6.02	36.12	36.12	31.74	36.12	36.12	27.46	0	36.12
	500	33.55	6.02	36.12	28.11	31.74	36.12	28.45	27.46	0

with

$$\sum_{B_x\in\{125,250,500\}} p_{(B_x|\,SF)} = 1, \quad \forall\, SF.$$

Using the ergodicity of the spatial PPP, this probability reduces to,

$$p_{(B_x|\,SF)} = \frac{|\mathcal{A}_{SF} \cap \mathcal{B}_{B_x}|}{|\mathcal{A}_{SF}|} \qquad (32)$$

with $|\mathcal{A}_{SF} \cap \mathcal{B}_{B_x}|$ and $|\mathcal{A}_{SF}|$ being the areas of $\mathcal{A}_{SF}\cap\mathcal{B}_{B_x}$ and $\mathcal{A}_{SF}$. Using (32), the delimiting outer radius of the $\mathcal{A}_{SF}\cap\mathcal{B}_{B_x}$ region can be computed as,

$$d^2_{(SF,B_x)} = \rho^2_{SF-1} + (\rho^2_{SF} - \rho^2_{SF-1}) \sum_{B_y\leq Bx} p_{(B_y|\,SF)}. \qquad (33)$$

The multi-channels assignment policy consists then in determining the values of the delimiting outer-radius $d_{(SF,B_x)}$ or equivalently $p_{(B_x|\,SF)}$ in order to minimize the worst case outage probability, *i.e.*,

$$\underset{p_{(B_x|\,SF)}}{\text{Minimize}}\ \bar{\mathbb{P}}_{\text{out}}. \qquad (34)$$

constrained by

$$\sum_{B_x\in\{125,250,500\}} p_{(B_x|\,SF)} = 1, \quad 7 \leq SF \leq 12.$$

Given the intensity of gateways and devices in the network, an exhaustive search solution for this optimization problem is provided in Section VI.

VI. NUMERICAL RESULTS

We consider a cellular LoRa network considering EU regional specifications in [4] with system parameters summarized in Table 1 studied in both cases of urban and rural environments. The density of active nodes ρ_a nodes per km^2 and per min transmitting in average n_a messages a day. In rural (respectively urban) environment, we set $n_a = 2$ (respectively $n_a = 8$) and $\rho_a = 72$ (respectively $\rho_a = 360$) nodes per km^2. We assume that the mean time of service is $\nu^{-1} = 12$s. The intensity of active nodes computed as $\lambda_a = n_a\rho_a\nu^{-1}/(24 \times 60 \times 60)$ nodes per km^2 is equal to 0.02 nodes per km^2 (respectively 0.4 nodes per km^2) in rural (respectively in urban) environment.

A. ASSESSMENT OF THEORETICAL RESULTS

We compare in Figure 3 the simulated average outage probability and the analytic expressions in (29) computed in rural and urban environments considering fixed and optimized adaptive sub-band allocation. We assume that the nodes in the network transmit with a maximal power of 14 dBm. The outer-radii of the SF regions are computed with respect to the gateway intensities λ_b as explained in Subsection V-A to distribute the spreading factors in the whole area of coverage. Considering the adaptive band policy, the outer-radius $d_{(SF,B_x)}$ of $\mathcal{A}_{SF} \cap \mathcal{B}_{B_x}$ is chosen for each gateway intensity case in order to minimize the average outage probability in the cell. An exhaustive search is performed and the values of
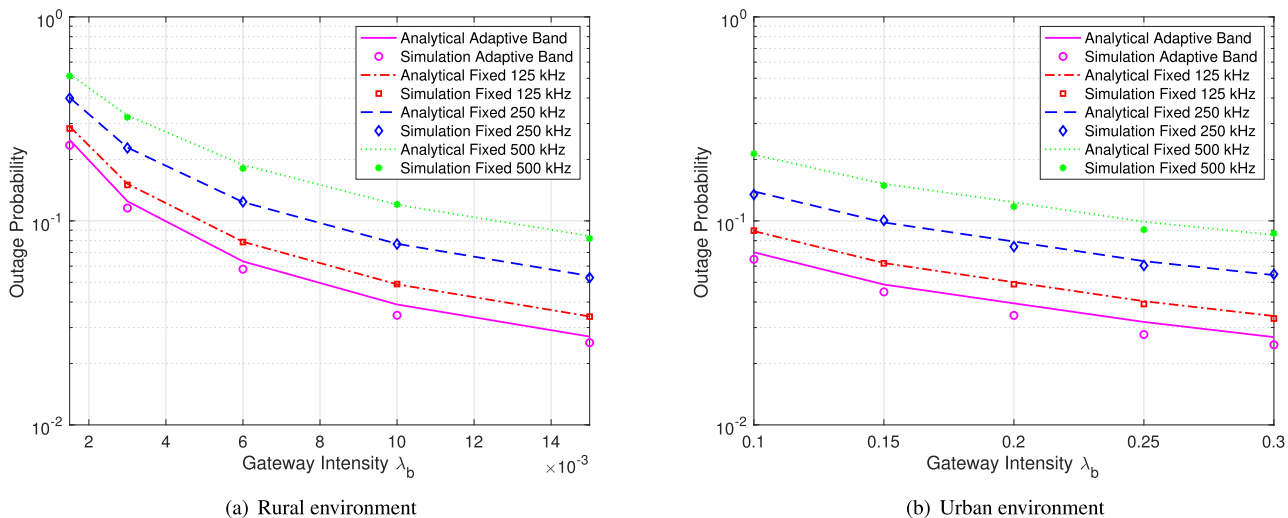
(a) Rural environment

(b) Urban environment

FIGURE 3. Comparison of analytic and simulation average outage probability computed with fixed and adaptive size of bandwidth.

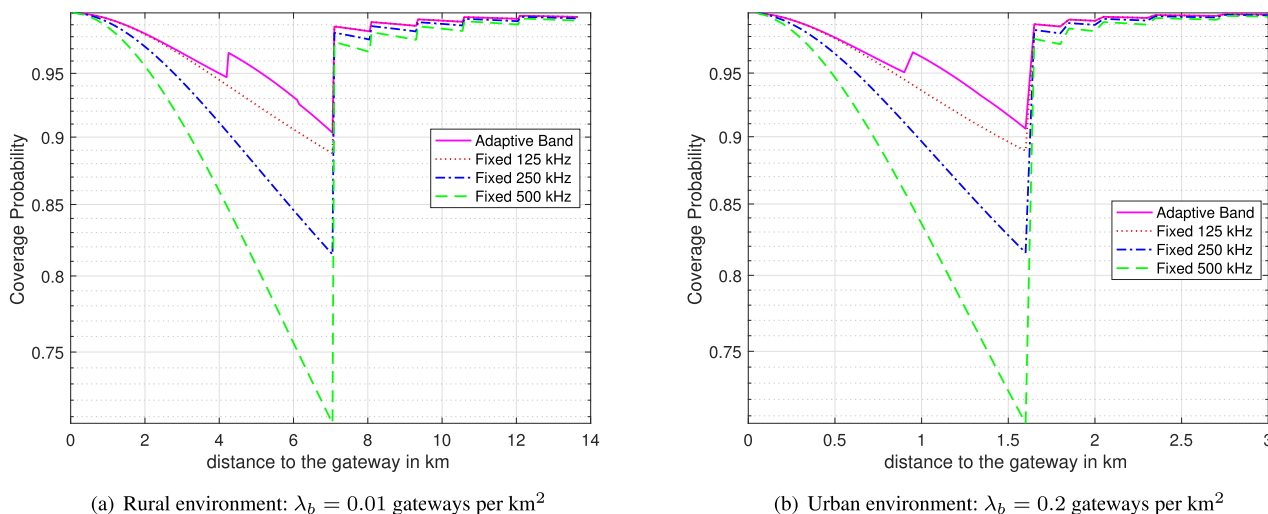(a) Rural environment: $\lambda_b = 0.01$ gateways per km^2

(b) Urban environment: $\lambda_b = 0.2$ gateways per km^2

FIGURE 4. Variation of coverage probability with distance.

the conditional probabilities $p_{(B_x \mid \mathrm{SF})}$ are determined. As we can see from Figures 3(a) and 3(b) corresponding respectively to urban and rural environments, the difference between the numerical and the analytic results is negligible which gives credit to our derived analytic results. For all policies, increasing the number of gateways reduces the size of the typical cells and enhances the level of the received SINR and consequently the outage probability. It can be observed from Figure 3(a) and 3(b) that increasing the size of the allocated fixed bandwidth increases the number of collision of the network. The interference level increases significantly and this cannot be compensated by the SINR threshold gain compared to the case of 125 kHz. For the adaptive band, the optimized choice of the outer-radius reduces the average outage probability compared to the fixed allocation policy. We can also notice that the outage probabilities have approximately the same ranges in rural and urban cases in

Figure 3(a) and 3(b). This is due to the compensation of the high interference level in the highly loaded urban cell, by the path-loss of long rural communication ranges.

B. COVERAGE PROBABILITY VARIATION
Figure 4 illustrates the variation of the coverage probability (complementary event as the outage one) with distance in rural and urban network. For both cases, we can see that the use of larger bandwidth is only advantageous for nodes situated in $\mathcal{A}_7$. For larger spreading factor, decreasing the spectral efficiency by increasing the size of the bandwidth does not over-balance the high level of interference on these bands coupled with the high inter-correlation factor between the lower spreading factor and lower bandwidth. For the urban and rural environments, we can note that for nodes with fixed band allocation situated at the edge of the region $\mathcal{A}_7$ with SF 7 are highly affected by the high level of interference
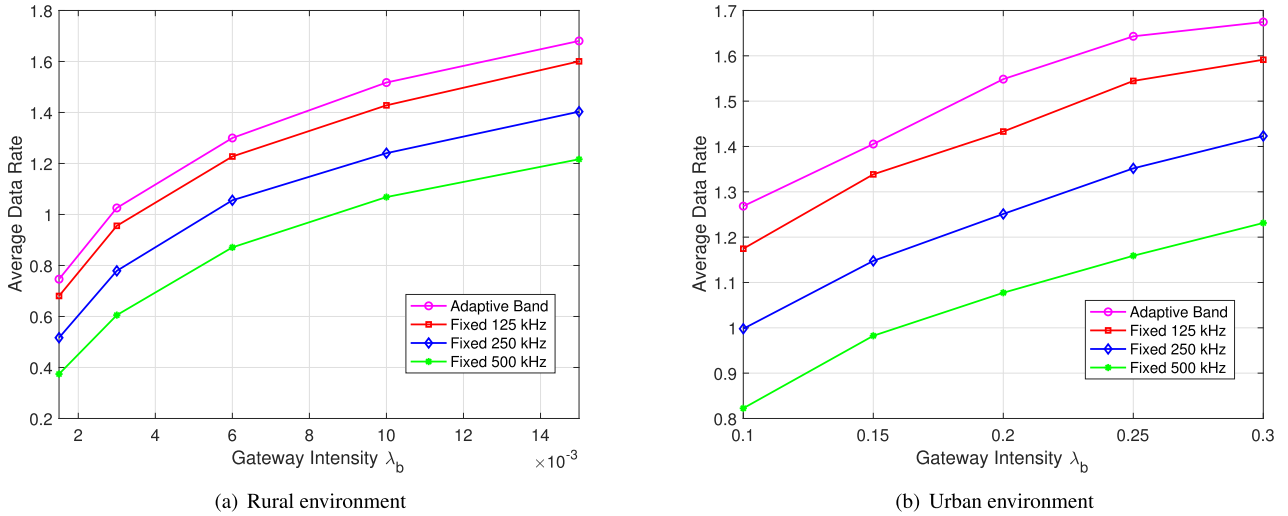
(a) Rural environment

(b) Urban environment

FIGURE 5. Average data rate in kbps versus the gateway intensities.

(a) Rural environment: $\lambda_b = 0.01$ gateways per km^2

(b) Urban environment: $\lambda_b = 0\,2$ gateways per km^2
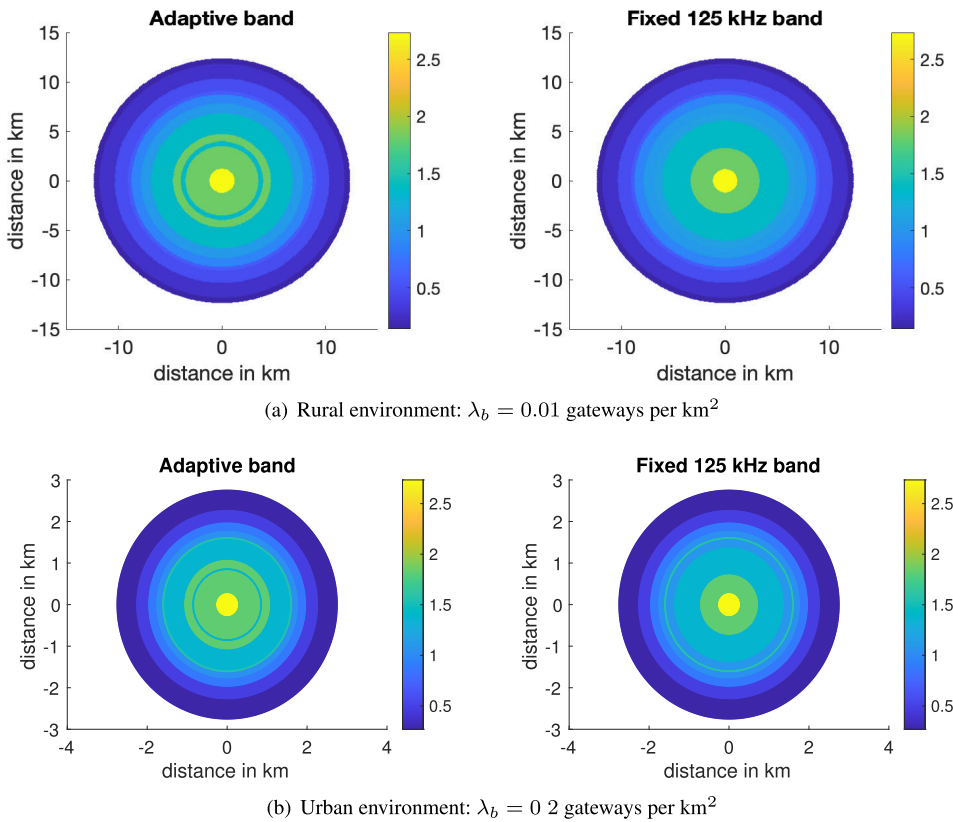
FIGURE 6. Rate distribution in kbps in the cell.

generated by nodes in the proximity of the gateway. In this case, several trials should be performed before achieving an acceptable successful transmission rate. The nodes that are situated in the higher SF zones do not face this problem as the inter-correlation factor between the higher SF order with the SF 7 region one is low. By using the above mentioned policy, we can notice that the progressive increase of the

bandwidth for nodes is only advantageous for nodes in the SF 7 region. The gain in SNR provided by the increase of the size of the bandwidth to 250 kHz in the network relatively counter-balance the high level of interference induced by the nodes in proximity to the gateway. Note as the channels overlap, the density of the interfering nodes on the 250 kHz becomes higher than if we kept the 125 kHz. However,
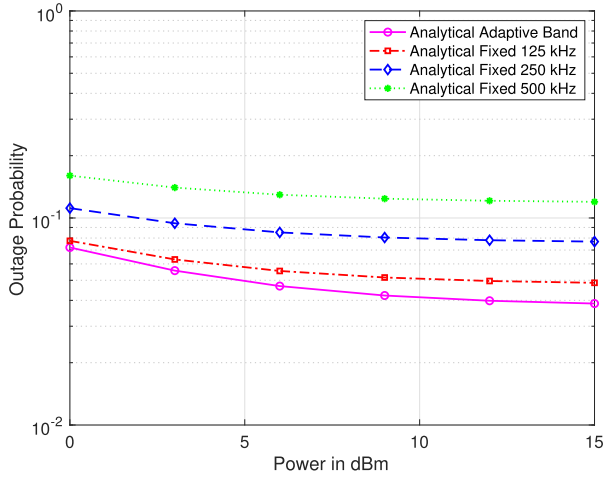
FIGURE 7. Outage probability versus the maximal transmitted power- Rural environment $\lambda_b = 0.01$ gateways per km^2.

FIGURE 8. Average data rate in kb/s versus the device power - Rural environment $\lambda_b = 0.01$ gateways per km^2.

the inter-correlation factor between the channels becomes lower and compensate for this high density. For the considered node intensity, the increase of the sub-band to 500 kHz is not benefiting as the inter-correlation factor does not compensate for the high density of interfering nodes.

C. AVERAGE DATA-RATE

Figure 5 compares the mean data rate considering rural and urban environments. We target a multiple trials outage probability of 10^{-4} achieved through several repetitions of the packet. These trials penalize the corresponding data rate related to each spreading factor. We can see that the adaptive band allocation policy slightly enhances the average data rate in the network compared to the other fixed band policies. Figure 6 compares the distribution of the rate in an urban and rural cell considering the adaptive and 125 kHz fixed allocation. In both cases, the adaptive band policy enhances the distribution of the rate in the zone with spreading factor of 7 which is naturally larger in the rural case than the urban one.

D. MAXIMAL TRANSMISSION POWER

Figure 7 illustrates the variation average outage probability considering long range rural communications in function of the maximal power of device. We can see that the adaptive band slightly enhances the power consumption compared to fixed band allocation. When targeting a single outage probability of 4×10^{-2} with a single trial, the required maximal probability with adaptive band is 12 dBm compared to 14 dBm with 125 kHz fixed band. The adaptive band allocation policy can enhance the maximal device power consumption.

Figure 8 shows the variation of the rate with the maximal transmitted power considering a multiple-trial threshold outage probability of 10^{-4}. We can see that for low power consumption, the data rate is much more penalized by the number of trials that should be performed. The adaptive allocation
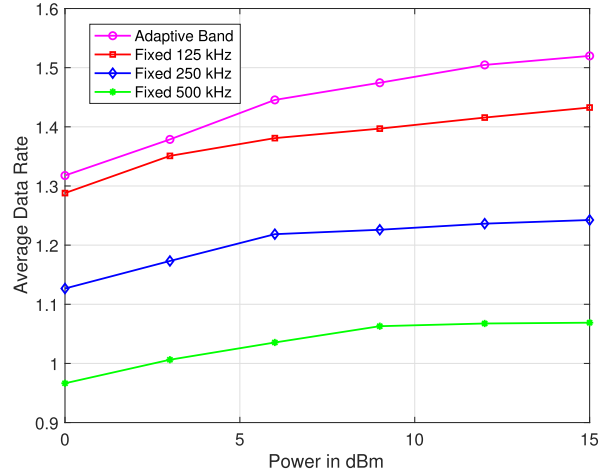
policy slightly enhances the data rate when increasing the power compared to other fixed allocation policies.

VII. CONCLUSION

In this paper, we proposed an adaptive bandwidth allocation policy compatible with the long range IoT LoRa networks specifications to mitigate the high interference level induced by nodes transmitting with the same SF. With respect to the distance to the station, a joint allocation of SF and one, two or four sub-channels of 125 kHz are allocated to a single sensor device. By modeling the network using spatial PPPs, we have statistically characterized an approximation of the interference Laplace transform in a typical cell taking into account the inter-correlation factor between the different spreading factors as well as the different allocated bandwidth. For this policy, we have derived the analytical expression of the outage probability. Based on this expression, we have computed in each SF region the outer-radius of the region where a larger bandwidth is required to minimize the average outage probability. We have shown that the optimized adaptive sub-band allocation outperforms the average outage probabilities with fixed allocation policy. Moreover, it minimizes the device power consumption and enhances the distribution of the rate in the cell by statistically decreasing the required number of trials for the edge nodes using the SF of 7. These results can be of high utility for network planners to find the dimensioning parameters of the network: the gateways' intensities, the maximal power consumption and to estimate the average data rate distribution in the network.

APPENDIX

A. INTERFERENCE LAPLACE TRANSFORM COMPUTATION

The interference Laplace transform is written as

$$\mathcal{L}_{I_x}(s) = \mathbb{E}\left[e^{-s\sum_{y\in\Phi_k} g(x,y)}\right] = \mathbb{E}\left[\prod_{y\in\Phi_k} e^{-sg(x,y)}\right].$$

with

$$g(x, y) = c(x, y)\alpha|y|^{-\beta}A_f P_t \prod_{z \in \Phi_b} \mathbb{1}_{\{|y| < |z-y|\}}.$$

Note that $c(x, y) = c_{\{SF_0, B_0, SF, B_0\}} \times \mathbb{1}_{\{y \in \mathcal{A}_{SF}\}}$ and $\mathcal{A}_{SF}$ being defined in (6).

Next, we rewrite $e^{-sg(x,y)}$ as,

$$e^{-sg(x,y)} = 1 - \left(1 - e^{-sc(x,y)\alpha|y|^{-\beta}A_f P_t}\right)\prod_{z \in \Phi_b} \mathbb{1}_{\{|y| < |z-y|\}}.$$

1) FIXED SUB-BAND ALLOCATION CASE

For the fixed sub-band allocation case, the interferers are distributed in an homogeneous PPP with intensity λ_a/N_m. By applying the Probability Generating Functional (PGFL) property,

$$\mathcal{L}_{I_x}(s) = \exp\left(-\frac{\lambda_a}{N_m}\mathbb{E}_z\left[\int \left(1 - e^{-sg(x,y)}\right)f(A_f)dA_f dy\right]\right),$$

with $f(A_f) = e^{-A_f}$ being the exponential distribution of A_f. Focusing now on the integral on the Right Hand Side (RHS), this latter can be written as,

RHS integral
$$= \int_0^\infty \int_0^{2\pi} \int_0^\infty \left(1 - e^{-sc(x,y)\alpha r^{-\beta}A_f P_t}\right)$$
$$\times \mathbb{E}_z\left[\prod_{z \in \Phi_b} \mathbb{1}_{\{|y| < |z-y|\}}\right]e^{-A_f} r dr \, d\theta \, dA_f \quad (35)$$

Once again, using the PGFL property, we have,

$$\mathbb{E}\left[\prod_{z \in \Phi_b} \mathbb{1}_{\{r < |z-y|\}}\right] = \exp\left(-\lambda_b\int_{\mathbb{R}^2}(1 - \mathbb{1}_{\{r < |z-y|\}})dz\right)$$
$$= \exp\left(-\lambda_b\int_{|z-y|^2 < r^2} dz\right). \quad (36)$$

Note that $|z-y| = |z|^2 + |y|^2 - 2|z||y|\cos(\theta_z - \theta_y)$ where $r_z = |z|$ and θ_z (resp. $r_y = r = |y|$ and θ_y) are the polar coordinates of z (resp. y). The condition $|z-y|^2 < r^2$ in (36) is then equivalent to $|z| < 2|y|\cos(\theta_z - \theta_y)$ such that $\cos(\theta_z - \theta_y) > 0$. The corresponding integral

$$\int_{|z-y|^2 < r^2} dz = \int_{\theta_y}^{\theta_y + \pi} \int_0^{2 r_y \cos(\theta_z - \theta_y)} r_z dr_z d\theta_z = \pi r_y^2.$$

Replacing $c(x, y)$ by its value, we can get the expression of $\mathcal{L}_{I_x}(s)$ in (23).

2) ADAPTIVE MULTI-CHANNELS ALLOCATION CASE

The main difference between the adaptive multi-channels and fixed sub-band allocation is the spatial distribution of the PPP that becomes heterogeneous. The intensity becomes then position dependent. The expression of the Laplace transform can be deduced by repeating similar steps as the fixed sub-band allocation case, and by taking into account the heterogeneity of the spatial PPP.

REFERENCES

[1] *Ericsson Website*. [Online]. Available: https://www.ericsson.com/assets/local/mobility-report/documents/2018/ericsson-mobility-report-june-2018.pdf

[2] *Semtech Website*. [Online]. Available: https://lora-developers.semtech.com/

[3] *LoRaWAN Specification*. [Online]. Available: https://lora-alliance.org/lorawan-for-developers

[4] *LoRaWAN Regional Parameters Specification*. LoRaWAN Regional Parameters Specification. [Online]. Available: https://lora-alliance.org/resource-hub/rp2-101-lorawanr-regional-parameters-0

[5] *LoRa Alliance Website*. [Online]. Available: https://lora-alliance.org/

[6] N. Jovalekic, V. Drndarevic, E. Pietrosemoli, and I. Zennaro, "Experimental study of LoRa transmission over seawater," *Sensors*, vol. 18, no. 9, p. 2853, Aug. 2018. [Online]. Available: http://www.mdpi.com/1424-8220/18/9/2853

[7] J. Gaelens, P. Van Torre, J. Verhaevert, and H. Rogier, "LoRa mobile-to-base-Station channel characterization in the antarctic," *Sensors*, vol. 17, no. 8, p. 1903, Aug. 2017. [Online]. Available: http://www.mdpi.com/1424-8220/17/8/1903

[8] J. Petäjäjärvi, K. Mikhaylov, M. Pettissalo, J. Janhunen, and J. Iinatti, "Performance of a low-power wide-area network based on LoRa technology: Doppler robustness, scalability, and coverage," *Int. J. Distrib. Sensor Netw.*, vol. 13, no. 3, Mar. 2017, Art. no. 155014771769941, doi: 10.1177/1550147717699412.

[9] A. Augustin, J. Yi, T. Clausen, and W. Townsley, "A study of LoRa: Long range & low power networks for the Internet of Things," *Sensors*, vol. 16, no. 9, p. 1466, Sep. 2016.

[10] T. Bouguera, J.-F. Diouris, J.-J. Chaillout, R. Jaouadi, and G. Andrieux, "Energy consumption model for sensor nodes based on LoRa and LoRaWAN," *Sensors*, vol. 18, no. 7, p. 2104, Jun. 2018, doi: 10.3390/s18072104.

[11] J. C. Liando, A. Gamage, A. W. Tengourtius, and M. Li, "Known and unknown facts of LoRa: Experiences from a large-scale measurement study," *ACM Trans. Sen. Netw.*, vol. 15, no. 2, pp. 16:1–16:35, Feb. 2019, doi: 10.1145/3293534.

[12] C. Goursaud and J. M. Gorce, "Dedicated networks for IoT: PHY / MAC state of the art and challenges," *EAI Endorsed Trans. Internet Things*, vol. 1, no. 1, Oct. 2015, Art. no. 150597.

[13] O. Georgiou and U. Raza, "Low power wide area network analysis: Can LoRa scale?" *IEEE Wireless Commun. Lett.*, vol. 6, no. 2, pp. 162–165, Apr. 2017.

[14] N. Sornin, M. Luis, T. Eirich, T. Kramp, and O. Hersent, "Lorawan specification," LoRa Alliance Tech. Rep., 2016.

[15] J. G. Andrews, A. K. Gupta, and H. S. Dhillon, "A primer on cellular network analysis using stochastic geometry," 2016, *arXiv:1604.03183*. [Online]. Available: https://arxiv.org/abs/1604.03183

[16] F. Baccelli and B. Blaszczyszyn, "Stochastic geometry and wireless networks: Theory," *Found. Trends Netw.*, vol. 1, no. 3, pp. 249–449, 2010.

[17] F. Baccelli and B. Blaszczyszyn, "Stochastic geometry and wireless networks:, Application," *Found. Trends Netw.*, vol. 2, no. 4, pp. 1–312, 2010.

[18] R. Giacomelli, R. K. Ganti, and M. Haenggi, "Outage probability of general ad hoc networks in the high-reliability regime," *IEEE/ACM Trans. Netw.*, vol. 19, no. 4, pp. 1151–1163, Aug. 2011.

[19] M. Haenggi, "Outage, local throughput, and capacity of random wireless networks," *IEEE Trans. Wireless Commun.*, vol. 8, no. 8, pp. 4350–4359, Aug. 2009.

[20] M. Haenggi and R. K. Ganti, "Interference in large wireless networks," *Found. Trends Netw.*, vol. 3, no. 2, pp. 127–248, 2008.

[21] S. Weber, J. G. Andrews, and N. Jindal, "An overview of the transmission capacity of wireless networks," *IEEE Trans. Commun.*, vol. 58, no. 12, pp. 3593–3604, Dec. 2010.

[22] S. P. Weber, X. Yang, J. G. Andrews, and G. deVeciana, "Transmission capacity of wireless ad hoc networks with outage constraints," *IEEE Trans. Inf. Theory*, vol. 51, no. 12, pp. 4091–4102, Dec. 2005.

[23] A. Springer, W. Gugler, M. Huemer, L. Reindl, C. C. W. Ruppel, and R. Weigel, "Spread spectrum communications using chirp signals," in *Proc. IEEE/AFCEA EUROCOMM Inf. Syst. Enhanced Public Saf. Secur.*, May 2000, pp. 166–170.

[24] G. Ferre and A. Giremus, "LoRa physical layer principle and performance analysis," in *Proc. 25th IEEE Int. Conf. Electron., Circuits Syst. (ICECS)*, Dec. 2018, pp. 65–68.

YI YU received the bachelor's degree in aerospace science and technology from Xidian University, Xi'an, China, in 2016, and the M.Sc. degree in telecommunication and network from Conservatoire National des Arts et Métiers (CNAM), Paris, France, in 2017. She is currently pursuing the Ph.D. degree with the Conservatoire National des Arts et Métiers (CNAM) and the Institut Supérieur d'Electronique de Paris (ISEP), Paris. Her main areas of research interests incude radiocommunications, the IoT networks, low power wide area network (LPWAN), and radio resources management.

GUILLAUME VIVIER (Senior Member, IEEE) received the M.Sc. degree in telecommunication engineering from Télécom Paris, Paris, France, in 1993, and the Ph.D. degree from the University of Pierre and Marie Curie, Paris, in 2003. After various positions with Alcatel and Motorola, he joined Sequans Communications to drive innovation into products. He is currently the Head of CTO Office. He coordinates standardization activities as well as Sequans research collaborations in European and National funded programs. He initiated 5G activity to prepare future generation of Sequans' chipsets.

LINA MROUEH (Member, IEEE) received the Engineering degree from Télécom Paris, in 2006, the M.Sc. degree from the University of Pierre and Marie Curie, in 2006, the Ph.D. degree from Télécom Paris, in 2010, and the Habilitation degree (to lead research) from Sorbonne University, in 2019. From 2006 to 2009, she worked as a Research Engineer with the Seamless Radio Laboratory, Motorola Labs. In 2009, she was a Visiting Student with the Communication Theory Group, ETH Zürich, where she was a Postdoctoral Student, in 2010. She is currently an Associate Professor with the Institut Supérieur d'Electronique de Paris (ISEP) and the Head of the Research Group in Electronics and Communications. Her research interests include the space time coding design for wireless and free space optical MIMO communications, radio resource allocation, and dimensioning in wireless networks.

JEAN-MARIE GORCE (Senior Member, IEEE) received the M.Sc. and Ph.D. degrees in electrical engineering from the Institut National des Sciences Appliquées (INSA) Lyon, France, in 1993 and 1998, respectively. He is currently a Professor at INSA, Université de Lyon, and he is a Research Member of the Institut National de Recherche en Informatique et en Automatique (INRIA). He was a Co-Founder of the Centre for Innovation in Telecommunications and Integration of Services (CITIlab), in 2001. He is currently the Vice Delegate for research at INRIA Grenoble, and he holds the Internet of Things Industrial and Research Chair of INSA Lyon sponsored by SPIE ICS. He was a Visiting Scholar at Princeton University, NJ, USA, from 2013 to 2014. He has co-published more than 150 conference and journal articles. His research interests include wireless networking and communication theory, focusing on realistic modeling, wireless system optimization, and performance assessment considering both infrastructure-based and ad hoc networks. He has been a principal investigator of several French and European sponsored projects related to wireless networks, and he is the Scientific Coordinator for the Experimental Facility FIT-CorteXlab. He is an Associate Editor of the *EURASIP Journal of Wireless Communications and Networking* (Springer).

DIANE DUCHEMIN (Member, IEEE) received the master's degree from the Telecommunication Department, INSA Lyon, France, in 2015, where she is currently pursuing the Ph.D. degree. She has been with the Center of Innovation in Telecommunications and Integration of service, INSA Lyon, as a Research Engineer on IoT Low Power Wide Area Networks. Her research interests include wireless communications and especially IoT LPWAN, non-orthogonal multiple access, compressive sensing, and multiple user's detection/estimation.

CLAIRE GOURSAUD (Member, IEEE) received the Ph.D. degree in high frequency and optical telecommunications from the University of Limoges, in 2006, working on signal processing for optical communications. In September 2007, she joined the INSA de Lyon (Institut National des Sciences Appliquées), as an Assistant Professor with the Telecommunication Department and the CITI Laboratory. She has published over 60 refereed journal and conference papers, and is an associate editor of two international journals. Her research interests include cooperation in wireless networks, and particularly on body area networks and the IoT UNB systems.

MICHEL TERRÉ received the Engineering degree from Télécom Sud Paris, in 1987, the Ph.D. degree from the Conservatoire National des Arts et Métiers (CNAM), in 1995, and the Habilitation à Diriger des Recherches (HDR) degree from Université Paris XIII, in 2004. He worked at Philips—Thales and Alcatel, from 1988 to 1998. He is currently a Full Professor at CNAM, Paris. He heads the research team in Electronics, Automatics and Signal Processing for Telecommunications (CEDRIC/Laetitia) at CNAM. His research areas include waveform optimization and blind channel estimation. He was the Co-Director of the European research project Phydyas, which proposed to use the FBMC approach for 5G. He is the author of more than 100 international articles and several patents. He is also the author of the online MATLAB code for generating an FBMC signal: ''ultraeasyFBMC.m'' which has been downloaded more than 2800 times.

• • •